Acta Mech 227, 3247–3260 (2016)
DOI 10.1007/s00707-015-1538-5

ORIGINAL PAPER

Williams R. Calderón-Muñoz · Cristian Jara-Bravo

Hydrodynamic modeling of hot-carrier effects in a PN junction solar cell

Received: 30 December 2014 / Revised: 14 August 2015 / Published online: 14 January 2016

Abstract This article presents a one-dimensional two-temperature hydrodynamic model to study the thermal and electrical behavior of a gallium arsenide (GaAs) PN junction solar cell. This model treats both electron and heat transfer on equal footing and includes Gauss's law, continuity and momentum equations for electrons and holes, and energy balance using temperature for both carriers and lattice. A zero-order system of equations is obtained using asymptotic series expansions based on the electron Reynolds number for steady-state conditions. An iterative scheme is implemented to solve the zero-order system. The results show the influence of carriers and lattice temperatures in the electrical performance of a GaAs PN junction solar cell. Higher values of power output are obtained with low lattice temperature and hot energy carriers. This modeling contributes to improve the thermal control in photovoltaic technologies.

1 Introduction

The third generation of solar cells has been developed with the goal of avoiding energy losses from different sources. While there are certain associated losses that cannot be reduced, such as black body radiation, some others such as spectrum losses, recombination processes or thermalization losses can be reduced by several techniques. The detailed balance limit of nearly 34 % considers a single-junction solar cell illuminated under concentrated light where each incoming photon excites one electron–hole pair (100 % quantum efficiency) and thermal energy of electrons over the conduction band is relaxed [1]. One of the means for improving this limit is multi-junction solar cells, which have several layers of semiconductors tuned to absorb a certain wavelength of light reaching a limit of efficiency of 42 % for a two-layer cell, 49 % for a three-layer cell and a theoretical limit of 68 % for an infinite-layer cell [2]. Another well-studied and currently operating technology is concentrator solar cells which benefit from requiring a reduced dimension and the relative low cost of concentrator lenses or mirrors. These cells are subjected to conditions of high radiation and require thermal control systems to achieve optimum performance. While multi-junction solar cells absorb radiation of different wavelengths, hot-carrier solar cells prevent the carriers from releasing its kinetic energy into lattice heating, permitting the transport of hot carriers and avoiding thermalization losses. Ideal hot-carrier solar cells have a detailed balance limit of

W. R. Calderón-Muñoz (✉) · C. Jara-Bravo
Department of Mechanical Engineering, Universidad de Chile, Beauchef 851, Santiago, Chile
E-mail: wicalder@ing.uchile.cl
Tel: +56-2-29784469
Fax: +56-2-26988453

C. Jara-Bravo
E-mail: crisjara@ing.uchile.cl

W. R. Calderón-Muñoz
Energy Center, Universidad de Chile, Tupper 2007, Santiago, Chile

85 % [3]. The main difficulty arises in thermally isolating carriers from phonons. In this sense, a mathematical model of hot-carrier transport can be useful to determine operating conditions that contribute to the reduction in thermalization losses.

Most of the modeling of semiconductor devices has been achieved through drift-diffusion models [4–6]. The main assumptions of these models are: (1) thermal equilibrium between charge carriers and lattice and (2) electron and hole populations each form a quasi-thermal equilibrium with a characteristic Fermi level and temperature [7]. Depletion region approximation, meaning the assumption of a region in a PN junction where carrier concentrations are considered negligible compared with doping concentrations (N_A and N_D), is also widely used. These approximations combined give a good understanding of the physical processes involved in PN junction semiconductor devices under particular circumstances. In the past decades, efforts have been made for expanding these models mainly because of the decrease in the device size (specially for transistors) and the increasing interest in new technologies for solar cells. In semiconductor modeling, hydrodynamic models have been used to describe the electron transport and temperature distributions in devices such as field effect transistors [8–13]. These models have also been used in the stability analysis of electron flow to understand whether semiconductors can be used as a radiative source [14,15], and lately to study the electron and hole transport in quantum wells [16,17]. Physical similarities with fluid flow have been found for electron flow in semiconductor devices by using hydrodynamic models [18]. From a thermal perspective, two-temperature models have been used to describe semiconductor and thermoelectric devices [19,20]. Hydrodynamic models permit to avoid details of the distribution of electrons and holes by providing a set of partial differential equations to describe the voltage, the evolution of the electron and hole velocities, densities and temperatures throughout the junction [21].

In this research, a one-dimensional two-temperature hydrodynamic model is used to simulate the steady-state operating conditions of a GaAs single PN junction solar cell used under light. The dependency of charge carrier and lattice temperature boundary conditions with power output is discussed.

2 Mathematical modeling and physical considerations

2.1 Governing equations

The definition of a hydrodynamic model for semiconductors is not restricted to a single system of equations, but refers to the similarity they have with the governing equations in fluid dynamics. The model presented here is derived from the Boltzmann transport equations (BTE). Current is driven through the device by a voltage difference, diffusion, generation and recombination processes between the two contacts at $x^* = 0, L$. The coordinate x^* is in the direction of the electron flow, and t^* is time. The one-dimensional two-temperature hydrodynamic equations for electron and hole flow in a PN junction solar cell include Gauss's law in Eqs. (1a) and (1b), mass conservation equations for electrons and holes in Eqs. (1c) and (1d), momentum conservation equations for electrons and holes in Eqs. (1e) and (1f) and energy conservation equation for electrons and lattice in Eqs. (1g) and (1h). We consider thermal equilibrium between electrons and holes. Therefore, the electron and hole temperature distributions are imposed to be equal throughout the device, T_c^*. The system of equations is

$$\frac{\partial^2 V^*}{\partial x^{*2}} = -\frac{e}{\varepsilon_s}\left(p^* - n^* - N_A\right), \quad x^* < x_J^*, \tag{1a}$$

$$\frac{\partial^2 V^*}{\partial x^{*2}} = -\frac{e}{\varepsilon_s}\left(p^* - n^* + N_D\right), \quad x^* > x_J^*, \tag{1b}$$

$$\frac{\partial n^*}{\partial t^*} + \frac{\partial (u_e^* n^*)}{\partial x^*} = (G_n^* - R_n^*), \tag{1c}$$

$$\frac{\partial p^*}{\partial t^*} + \frac{\partial (u_h^* p^*)}{\partial x^*} = (G_p^* - R_p^*), \tag{1d}$$

$$\frac{\partial u_e^*}{\partial t^*} + u_e^* \frac{\partial u_e^*}{\partial x^*} = \frac{e}{m_e}\frac{\partial V^*}{\partial x^*} - \frac{k_B}{m_e n^*}\frac{\partial (n^* T_c^*)}{\partial x^*} - \frac{u_e^*}{\tau_{el}}, \tag{1e}$$

$$\frac{\partial u_h^*}{\partial t^*} + u_h^* \frac{\partial u_h^*}{\partial x^*} = -\frac{e}{m_h}\frac{\partial V^*}{\partial x^*} - \frac{k_B}{m_h p^*}\frac{\partial (p^* T_c^*)}{\partial x^*} - \frac{u_h^*}{\tau_{hl}}, \tag{1f}$$

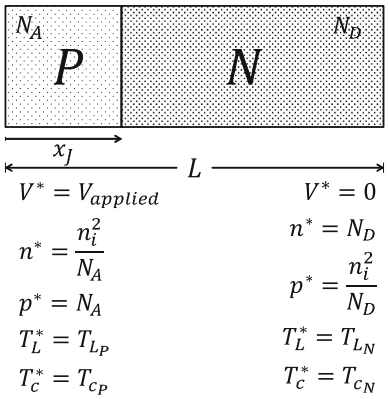

Fig. 1 Device scheme with boundary conditions

$$\frac{\partial T_c^*}{\partial t^*} + u_e^* \frac{\partial T_c^*}{\partial x^*} = -\frac{2}{3} T_c^* \frac{\partial u_e^*}{\partial x^*} + \frac{2}{3n^* k_B} \frac{\partial}{\partial x^*} \left(k_e \frac{\partial T_c^*}{\partial x^*} \right) - \frac{T_c^* - T_L^*}{\tau_E} + \frac{2m_e}{3k_B \tau_{el}} \left(u_e^{*2} - \frac{\tau_{el}}{2\tau_E} (u_e^{*2} - u_h^{*2}) \right), \tag{1g}$$

$$C_L \frac{\partial T_L^*}{\partial t^*} = \frac{\partial}{\partial x^*} \left(k_L \frac{\partial T_L^*}{\partial x^*} \right) + \frac{3n^* k_B}{2} \left(\frac{T_c^* - T_L^*}{\tau_E} \right) + \frac{n^* m_e}{2\tau_E} \left(u_e^{*2} \right) + \frac{3p^* k_B}{2} \left(\frac{T_c^* - T_L^*}{\tau_E} \right) + \frac{p^* m_h}{2\tau_E} \left(u_h^{*2} \right), \tag{1h}$$

where $V^*(x^*, t^*)$ is the voltage, $n^*(x^*, t^*)$ is the electron density, $p^*(x^*, t^*)$ is the hole density, $u_e^*(x^*, t^*)$ is the x^*-component electron drift velocity, $u_h^*(x^*, t^*)$ is the x^*-component hole drift velocity, T_c^* is the carrier temperature and T_L^* is the lattice temperature. The junction is defined at $x^* = x_J^*$.

The physical parameters are the electron charge, e, the permittivity of the semiconductor, ε_s, the donor concentration, N_D, the acceptor concentration, N_A, the effective electron mass, m_e, the effective hole mass, m_h, the electron–hole reduced mass μ_{eh}, the Boltzmann constant, k_B, the generation rate for electrons, G_n, the generation rate for holes, G_p, the recombination rate for electrons, R_n, the recombination rate for holes, R_p, the momentum relaxation time for electrons, τ_{el}, the momentum relaxation time for holes, τ_{hl}, the relaxation time for electron–hole collisions, τ_{eh}, the energy relaxation time for electrons, τ_E, and the thermal conductivity for electrons, k_e.

The electric field, electron density and hole density at both ends are prescribed boundary conditions. The physical realization is by considering the both ends sufficiently far away from the junction, in the neutral regions. The carrier temperature, $T_c^* = T_e^* = T_h^*$, takes into account the thermal equilibrium between electrons and holes. Mathematically, the boundary conditions are $V^*(0, t^*) = V_{ap}$, $V^*(L, t^*) = 0$, $n^*(0, t^*) = n_i^2/N_A$, $n^*(L, t^*) = N_D$, $p^*(0, t^*) = N_A$, $p^*(L, t^*) = n_i^2/N_D$, $T_c^*(0, t^*) = T_{c_P}$, $T_c^*(L, t^*) = T_{c_N}$, $T_L^*(0, t^*) = T_{L_P}$, $T_L^*(L, t^*) = T_{L_N}$, where L is the length of the device and n_i is the intrinsic carrier concentration. We consider $T_{c_N} = T_{c_P}$ and $T_{L_N} = T_{L_P}$ as given temperatures for the carriers and lattice at the P and N sides, respectively, and V_{ap} as the applied voltage. The built-in potential of the PN junction is considered as a correction of the applied voltage and is considered for numerical calculations. The use of symmetric boundary conditions for the lattice and carrier temperatures is supported by the fact that the results from thermal modeling of photovoltaic solar cells show that the temperature of the semiconductor layer is mostly uniform along the normal axis [22]. The device scheme with boundary conditions is shown in Fig. 1. Since we are satisfying that the number of boundary conditions is the same as the order of the system of equations (1), we have a well-posed PDE mathematical problem.

For convenience, non-dimensional versions of the governing equations are obtained. By writing $V = V^*/V_0$, $n = n^*/N_0$, $p = p^*/N_0$, $x = x^*/L$, $u_e = u_e^*/U$, $u_h = u_h^*/U$, $T_c = T_c^*/T_0$, $T_L = T_L^*/T_0$ and $t = t^*U/L$, with V_0 is the reference voltage, N_0 is the reference doping density and T_0 is the reference temperature, the non-dimensional version of Eq. (1) is:

$$\frac{\partial^2 V}{\partial x^2} = -\alpha \left(p - n - \frac{N_A}{N_0} \right), \quad x < x_J, \tag{2a}$$

Table 1 Physical properties for GaAs [20,21]

Constant	Value
e	1.60218×10^{-19} C
ε_s	113.28×10^{-12} C^2/(N m^2)
k_B	1.38066×10^{-23} J/K
k_L	42.61 W/(m K)
N_D	1×10^{16} cm^{-3}
N_A	1×10^{17} cm^{-3}
m_e	6.01×10^{-32} kg
m_h	4.65×10^{-31} kg
C_L	8.73×10^{5} J/(m^3 K)
μ_{no}	0.45 m^2/(V s)
τ_p	2×10^{-12} s
τ_E	4.4×10^{-10} s

$$\frac{\partial^2 V}{\partial x^2} = -\alpha\left(p - n + \frac{N_D}{N_0}\right), \quad x > x_J, \tag{2b}$$

$$\frac{\partial n}{\partial t} + \frac{\partial (u_e n)}{\partial x} = (G_n - R_n), \tag{2c}$$

$$\frac{\partial p}{\partial t} + \frac{\partial (u_h p)}{\partial x} = (G_p - R_p), \tag{2d}$$

$$R_e\left[\frac{\partial u_e}{\partial t} + u_e\frac{\partial u_e}{\partial x}\right] = \frac{\partial V}{\partial x} - \frac{\beta}{n}\frac{\partial (nT_c)}{\partial x} - u_e, \tag{2e}$$

$$R_e\left[\frac{\partial u_h}{\partial t} + u_h\frac{\partial u_h}{\partial x}\right] = -m_r\left[\frac{\partial V}{\partial x} + \frac{\beta}{p}\frac{\partial (pT_c)}{\partial x}\right] - \gamma u_h, \tag{2f}$$

$$R_e\left[\frac{\partial T_c}{\partial t} + u_e\frac{\partial T_c}{\partial x} + \frac{2}{3}T_c\frac{\partial u_e}{\partial x}\right] = \phi_1\frac{1}{n}\frac{\partial^2 T_c}{\partial x^2} - \nu(T_c - T_L) + \phi_2\left(u_e^2 - \frac{\nu}{2}(u_e^2 - u_h^2)\right), \tag{2g}$$

$$\psi_0\frac{\partial T_L}{\partial t} = \psi_1\frac{\partial^2 T_L}{\partial x^2} + \nu(n+p)(T_c - T_L) + \psi_2\nu n u_e^2 + \frac{\psi_2}{m_r}\nu p u_h^2, \tag{2h}$$

where $\alpha = eL^2N_0/V_0\varepsilon_s$, $\gamma = \tau_{el}/\tau_{hl}$, $m_r = m_e/m_h$, $\beta = k_BT_0/eV_0$, $\nu = \tau_{el}/\tau_E$, $\phi_1 = (2k_e\tau_{el})/(3N_0k_BL^2)$, $\phi_2 = (2e^2V_0^2\tau_{el}^2)/(3m_ek_BT_0L^2)$, $\psi_0 = (2\tau_{el}C_LU)/(3N_0k_BL)$, $\psi_1 = (2\tau_{el}k_L)/(3N_0k_BL^2)$, $\psi_2 = (m_eU^2)/(3k_BT_0)$, $R_e = U^2m_e/eV_0$, $G_n - R_n = (G_n^* - R_n^*)L/N_0U$, $G_p - R_p = (G_p^* - R_p^*)L/N_0U$, and $U = eV_0\tau_{el}/m_eL$ is the maximum average electron velocity. R_e is the Reynolds number and it can be written as $R_e = U\tau_{el}/L$, which is the Knudsen number for the electron cloud.

2.2 Mathematical and numerical method

A one-dimensional two-temperature hydrodynamic model is used to simulate the steady-state operating conditions of a GaAs single PN junction solar cell used under concentrated light, in order to study the behavior of these devices when carriers are not in thermal equilibrium with lattice. Charge carrier densities, velocities, voltage and electric field distributions are obtained for different applied bias, and the total current densities (electrons and holes) as a function of applied voltage are obtained for different carrier temperature boundary conditions. We consider the physical properties for GaAs given in Table 1, the system parameters given in Table 2 and the non-dimensional parameters given in Table 3. For the purposes of this paper, a PN junction under light (constant net generation rate) with $x_J = 0.1$ was considered. Since Eq. (2) are nonlinear, we use perturbation method in asymptotic expansions to reduce the nonlinearities and get an approximated solution [23].

If the number of collisions in the device is high, it is expected to have a small distance between two collisions for an electron in the flow. This assumption implies that the Reynolds number is small $R_e < 1$, and it can be used as a perturbation parameter in asymptotic perturbation series for the dependent variables in Eqs. (2). The asymptotic perturbation series for the dependent variables are

Table 2 System parameters

Constant	Value
L	10×10^{-6} m
N_0	1×10^{16} cm^{-3}
V_0	1.0 V
T_0	300 K

Table 3 Dimensionless parameters for GaAs

Parameter	Value
α	1403
β	0.026
γ	1.118
m_r	0.129
ν	0.357
ψ_1	0.397
ψ_2	0.017
ϕ_1	0.031
ϕ_2	0.034
R_e	1.3×10^{-3}

$$
\begin{aligned}
\overline{V}(x) &\approx \overline{V}_0(x) + \varepsilon \overline{V}_1(x) + \cdots, \\
\overline{n}(x) &\approx \overline{n}_0(x) + \varepsilon \overline{n}_1(x) + \cdots, \\
\overline{p}(x) &\approx \overline{p}_0(x) + \varepsilon \overline{p}_1(x) + \cdots, \\
\overline{u}_e(x) &\approx \overline{u_{e0}}(x) + \varepsilon \overline{u_{e1}}(x) + \cdots, \\
\overline{u}_h(x) &\approx \overline{u_{h0}}(x) + \varepsilon \overline{u_{h1}}(x) + \cdots, \\
\overline{T}_c(x) &\approx \overline{T_{c0}}(x) + \varepsilon \overline{T_{c1}}(x) + \cdots, \\
\overline{T}_L(x) &\approx \overline{T_{L0}}(x) + \varepsilon \overline{T_{L1}}(x) + \cdots,
\end{aligned}
$$

where $\varepsilon = R_e$. By replacing the asymptotic expansions into the steady-state version of Eq. (2), a zero-order system is obtained. This system can be written in terms of electron and hole current densities. Two second-order differential equations for the electron and hole densities are obtained by combining the continuity and momentum conservation equations:

$$\frac{d^2\overline{V}_0}{\mathrm{d}x^2} = -\alpha\left(\overline{p}_0 - \overline{n}_0 - \frac{N_A}{N_0}\right), \quad x < x_J, \tag{3a}$$

$$\frac{d^2\overline{V}_0}{\mathrm{d}x^2} = -\alpha\left(\overline{p}_0 - \overline{n}_0 + \frac{N_D}{N_0}\right), \quad x > x_J, \tag{3b}$$

$$\beta\frac{d^2(\overline{n}_0\overline{T}_{c0})}{\mathrm{d}x^2} - \frac{d\overline{n}_0}{\mathrm{d}x}\frac{d\overline{V}_0}{\mathrm{d}x} - \overline{n}_0\frac{\mathrm{d}^2\overline{V}_0}{\mathrm{d}x^2} + (G_n - R_n) = 0, \tag{3c}$$

$$\beta\frac{d^2(\overline{p}_0\overline{T}_{c0})}{\mathrm{d}x^2} + \frac{d\overline{p}_0}{\mathrm{d}x}\frac{d\overline{V}_0}{\mathrm{d}x} + \overline{p}_0\frac{\mathrm{d}^2\overline{V}_0}{\mathrm{d}x^2} + \frac{\gamma}{m_r}(G_p - R_p) = 0, \tag{3d}$$

$$\phi_1\frac{d^2\overline{T}_{c0}}{\mathrm{d}x^2} - \nu\overline{n}_0(\overline{T}_{c0} - \overline{T}_{L0}) + \phi_2\overline{n}_0\left(\overline{u}_{e_0}^2 - \frac{\nu}{2}(\overline{u}_{e_0}^2 - \overline{u}_{h_0}^2)\right) = 0, \tag{3e}$$

$$\psi_1\frac{d^2\overline{T}_{L0}}{\mathrm{d}x^2} + \nu(\overline{n}_0 + \overline{p}_0)(\overline{T}_{c0} - \overline{T}_{L0}) + \psi_2\nu\overline{n}_0\overline{u}_{e_0}^2 + \frac{\psi_2}{m_r}\nu\overline{p}_0\overline{u}_{h_0}^2 = 0, \tag{3f}$$

where

$$\overline{u_{e0}} = \frac{d\overline{V}_0}{\mathrm{d}x} - \frac{\beta}{\overline{n}_0}\frac{d(\overline{n}_0\overline{T}_{c0})}{\mathrm{d}x}, \tag{4a}$$

$$\overline{u_{h0}} = -\frac{m_r}{\gamma}\left(\frac{d\overline{V}_0}{\mathrm{d}x} + \frac{\beta}{\overline{p}_0}\frac{d(\overline{p}_0\overline{T}_{c0})}{\mathrm{d}x}\right). \tag{4b}$$

An iterative scheme is required to solve the zero-order system in Eqs. (3) due to the nonlinearities. For this, the finite difference method is used to discretize each equation separately assuming every variable known except for the one to obtain. Some input variables need to be chosen as initial conditions to solve the system in an explicit way from these conditions to the final steady-state conditions, moving forward by a pseudo-time step (θ) to obtain convergence. The iterative scheme was implemented in the software Wolfram Mathematica.

The voltage, $\overline{V}_0(x)$, and carrier temperature, $\overline{T_{c0}}(x)$, are used as initial conditions. A linear distribution is used for carrier temperature between boundary conditions, giving

$$\overline{T_{c0}}^0(x) = T_{cN} + (T_{cN} - T_{cP})x, \tag{5}$$

where $x \in [0, 1]$, since it is the normalized length. The depletion region approximation [5] is used to determine the initial condition of the voltage. For simplicity, the depletion region length is obtained for the P- and N-doped sides of the junction as dimensionless values, w_n and w_p, respectively:

$$w_p = \left[\frac{2\varepsilon_s(V_{bi} - V_{app})}{qL^2}\left(\frac{N_A}{N_D(N_A + N_D)}\right)\right]^{1/2}, \tag{6}$$

$$w_n = \left[\frac{2\varepsilon_s(V_{bi} - V_{app})}{qL^2}\left(\frac{N_D}{N_A(N_A + N_D)}\right)\right]^{1/2}. \tag{7}$$

Using these expressions, the depletion region approximation for voltage is obtained as a combination of parabolic profiles resulting from the integration of the depleted regions.

$$\overline{V}_0^0(x) = \begin{cases} V_P & 0 < x < w_p, \\ \left(qN_AL^2/\varepsilon_sV_0\right)\left((x - x_J)^2 + 2w_p(x - x_J) + w_p^2\right) + V_P & w_p < x < x_J, \\ \left(qN_DL^2/\varepsilon_sV_0\right)\left((x - x_J)^2 + 2w_n(x - x_J) - w_n^2\right) + V_N & x_J < x < x_J + w_n, \\ V_N & x_J + w_n < x < 1. \end{cases} \tag{8}$$

The second-order equation for the electron density, Eq. (3c), can be written for the iteration step k as

$$\frac{d^2\overline{n}_0^k}{dx^2}\lambda_{n_1} + \frac{d\overline{n}_0^k}{\mathrm{d}x}\lambda_{n_2} + \overline{n}_0^k\lambda_{n_3} = (R_n - G_n), \tag{9}$$

where $\lambda_{n_1} = \beta\overline{T_{c_0}}^k$, $\lambda_{n_2} = 2\beta(d\overline{T_{c_0}}^k/\mathrm{d}x) - (d\overline{V_0}^k/\mathrm{d}x)$ and $\lambda_{n_3} = \beta(d^2\overline{T_{c_0}}^k/\mathrm{d}x^2) - (d^2\overline{V_0}^k/\mathrm{d}x^2)$. A regular one-dimensional grid is used with a spatial step size of Δx. An upwind scheme was used to discretize the first-order derivatives, and therefore, the direction of the discretization depends on the sign of λ_{n_2} in the way described below where the notation $z(\mathrm{step}_k, x_i) = z_i^k$ is considered:

$$\frac{d(\overline{n}_0)_i^k}{\mathrm{d}x} = \begin{cases} \left((\overline{n}_0)_{i+1}^k - (\overline{n}_0)_i^k\right)/\Delta x & \text{if } (\lambda_{n_2})_i < 0 \\ \left((\overline{n}_0)_i^k - (\overline{n}_0)_{i-1}^k\right)/\Delta x & \text{if } (\lambda_{n_2})_i > 0 \end{cases} \tag{10}$$

From this, the discretized equation can be expressed as a linear system in matrix form, where the diagonal of a tridiagonal matrix is defined as

$$(A_n)_{ii} = \begin{cases} -2(\lambda_{n_1})_i/\Delta x^2 - (\lambda_{n_2})_i/\Delta x + (\lambda_{n_3})_i & \text{if } (\lambda_{n_2})_i < 0, \\ -2(\lambda_{n_1})_i/\Delta x^2 + (\lambda_{n_2})_i/\Delta x + (\lambda_{n_3})_i & \text{if } (\lambda_{n_2})_i > 0. \end{cases} \tag{11}$$

The superdiagonal and subdiagonal are defined in a similar way as

$$(A_n)_{ij|(i-j)=-1} = \begin{cases} (\lambda_{n_1})_i/\Delta x^2 + (\lambda_{n_2})_i/\Delta x & \text{if } (\lambda_{n_2})_i < 0, \\ (\lambda_{n_1})_i/\Delta x^2 & \text{if } (\lambda_{n_2})_i > 0, \end{cases} \tag{12}$$

$$(A_n)_{ij|(i-j)=1} = \begin{cases} (\lambda_{n_1})_i/\Delta x^2 & \text{if } (\lambda_{n_2})_i < 0, \\ (\lambda_{n_1})_i/\Delta x^2 - (\lambda_{n_2})_i/\Delta x & \text{if } (\lambda_{n_2})_i > 0. \end{cases} \tag{13}$$

Therefore, the right hand side of the system is

$$(f_n)_i = (R_n - G_n)_i. \tag{14}$$

Finally, the linear system to solve in order to obtain the kth iteration step becomes

$$A_n(\overline{T}_{c0}^k, \overline{V}_0^k)\overline{n}_0^k = f_n. \tag{15}$$

The methodology to solve the second-order equation for the hole density, Eq. (3d), is analogue to the one used for Eq. (3c). Rewriting Eq. (3d), we get

$$\frac{d^2\overline{p}_0^k}{\mathrm{d}x^2}\lambda_{p_1} + \frac{d\overline{p}_0^k}{\mathrm{d}x}\lambda_{p_2} + \overline{p}_0^k\lambda_{p_3} = \frac{\gamma}{m_r}(R_p - G_p), \tag{16}$$

where $\lambda_{p_1} = \beta\overline{T}_{c0}^k, \lambda_{p_2} = 2\beta(d\overline{T}_{c0}^k/\mathrm{d}x) + (d\overline{V}_0^k/dx)$ and $\lambda_{p_3} = \beta(d^2\overline{T}_{c0}^k/\mathrm{d}x^2) + (d^2\overline{V}_0^k/\mathrm{d}x^2)$. The first-order discretization to be used is

$$\frac{d(\overline{p}_0)_i^k}{dx} = \begin{cases} \left((\overline{p}_0)_{i+1}^k - (\overline{p}_0)_i^k\right)/\Delta x & \text{if } (\lambda_{p_2})_i < 0, \\ \left((\overline{p}_0)_i^k - (\overline{p}_0)_{i-1}^k\right)/\Delta x & \text{if } (\lambda_{p_2})_i > 0. \end{cases} \tag{17}$$

The tridiagonal matrix to obtain the hole density can be expressed as

$$(A_p)_{ii} = \begin{cases} -2(\lambda_{p_1})_i/\Delta x^2 - (\lambda_{p_2})_i/\Delta x + (\lambda_{p_3})_i & \text{if } (\lambda_{p_2})_i < 0, \\ -2(\lambda_{p_1})_i/\Delta x^2 + (\lambda_{p_2})_i/\Delta x + (\lambda_{p_3})_i & \text{if } (\lambda_{p_2})_i > 0, \end{cases} \tag{18}$$

$$(A_p)_{ij|(i-j)=-1} = \begin{cases} (\lambda_{p_1})_i/\Delta x^2 + (\lambda_{p_2})_i/\Delta x & \text{if } (\lambda_{p_2})_i < 0, \\ (\lambda_{p_1})_i/\Delta x^2 & \text{if } (\lambda_{p_2})_i > 0, \end{cases} \tag{19}$$

$$(A_p)_{ij|(i-j)=1} = \begin{cases} (\lambda_{p_1})_i/\Delta x^2 & \text{if } (\lambda_{p_2})_i < 0, \\ (\lambda_{p_1})_i/\Delta x^2 - (\lambda_{p_2})_i/\Delta x & \text{if } (\lambda_{p2})_i > 0, \end{cases} \tag{20}$$

and the right-side vector is

$$(f_p)_i = \frac{\gamma}{m_r}(R_p - G_p)_i. \tag{21}$$

Finally, the linear system to solve in order to obtain the kth iteration step for holes becomes

$$A_p(\overline{T_{c_0}}^k, \overline{V_0}^k)\overline{p_0}^k = f_p. \tag{22}$$

Once the electron and hole densities are obtained, the velocities for electrons and holes along the device, $\overline{u}_{e_0}$ and $\overline{u}_{h_0}$ are obtained from Eqs. (4a) and (4b), respectively:

$$\overline{u_{e0}}^k(\overline{n}_0^k, \overline{V}_0^k, \overline{T}_{c0}^k) = \frac{d\overline{V}_0^k}{\mathrm{d}x} - \frac{\beta}{\overline{n}_0^k}\frac{d(\overline{n}_0^k\overline{T}_{c0}^k)}{\mathrm{d}x}, \tag{23}$$

$$\overline{u_{h0}}^k(\overline{p}_0^k, \overline{V}_0^k, \overline{T}_{c0}^k) = -\frac{m_r}{\gamma}\left(\frac{d\overline{V}_0^k}{\mathrm{d}x} + \frac{\beta}{\overline{p}_0^k}\frac{d(\overline{p}_0^k\overline{T}_{c0}^k)}{\mathrm{d}x}\right). \tag{24}$$

The next step is to solve the energy equation for lattice temperature, Eq. (3f), which can be written as

$$\psi_1\frac{d^2\overline{T}_{L0}^k}{\mathrm{d}x^2} + \nu\left(\overline{n}_0^k + \overline{p}_0^k\right)\left(\overline{T}_{c0}^k - \overline{T}_{L0}^k\right) + \psi_2\nu\overline{n}_0^k(\overline{u}_{e0}^k)^2 + \frac{\psi_2}{m_r}\nu\overline{p}_0^k(\overline{u}_{h0}^k)^2 = 0. \tag{25}$$

The lattice temperature profile $\overline{T}_{L0}^k(\overline{n}_0^k, \overline{p}_0^k, \overline{V}_0^k, \overline{T}_{c0}^k)$ can be easily obtained by solving the system of equations

$$A_L(\overline{n}_0^k)\overline{T}_{L0}^k = f_L(\overline{n}_0^k, \overline{p}_0^k, \overline{u}_{e0}^k, \overline{u}_{h0}^k), \tag{26}$$

where

$$(A_L)_{ij} = \begin{cases} -2\psi_1/\Delta x^2 - \nu\left((\overline{n}_0)_i^k + (\overline{p}_0)_i^k\right) & \text{if } i = j, \\ \psi_1/\Delta x^2 & \text{if } |i-j| = 1, \end{cases} \tag{27}$$

and

$$(f_L)_i(\overline{n}_0^k, \overline{p}_0^k, \overline{u_{e0}}^k, \overline{u_{h0}}^k) = -\psi_2 \nu \overline{n}_{0i}^k (\overline{u_{e0}}_i^k)^2 - \frac{\psi_2}{m_r}\nu \overline{p}_{0i}^k (\overline{u_{h0}}_i^k)^2 - \nu\left((\overline{n}_0)_i^k + (\overline{p}_0)_i^k\right)\overline{T_{c0}}_i^k. \tag{28}$$

An auxiliary iteration step is defined, k', before obtaining the new input variables for iteration step $k+1$. This is done by solving Poisson's equation and the energy equation for carriers, Eq. (3e), using the values for the other variables obtained in the kth iteration. Poisson's equation, Eqs. (3a) and (3b), can be written as

$$\frac{d^2\overline{V}_0^{k'}}{dx^2} = -\alpha\left(\overline{p}_0^k - \overline{n}_0^k + C\right), \tag{29}$$

where $C = -N_A/N_0$ in the P-side and $C = N_D/N_0$ in the N-side of the junction. Defining

$$(M_V)_{ij} = \begin{cases} -2 & \text{if } i = j, \\ 1 & \text{if } |i-j| = 1, \end{cases} \tag{30}$$

$$(f_V)_i(\overline{n}_0^k, \overline{p}_0^k) = -\alpha\left(\overline{p}_{0i}^k - \overline{n}_{0i}^k + C_i\right), \tag{31}$$

the new value $V_0^{k'}(\overline{n}_0^k, \overline{p}_0^k)$ is obtained by solving

$$M_V V_0^{k'} = f_V(\overline{n}_0^k, \overline{p}_0^k). \tag{32}$$

The energy equation for the carrier temperature, Eq. (3e), can be written as

$$\phi_1 \frac{d^2\overline{T_{c0}}^{k'}}{\mathrm{d}x^2} - \nu\overline{n}_0^k\left(\overline{T_{c0}}^{k'} - \overline{T_{L0}}^k\right) + \phi_2\left((\overline{u_{e0}}^k)^2 - \frac{\nu}{2}\left((\overline{u_{e0}}^k)^2 - (\overline{u_{h0}}^k)^2\right)\right) = 0 \tag{33}$$

to obtain $\overline{T_{c0}}^{k'}(\overline{n}_0^k, \overline{T_{L0}}^k, \overline{u_{e0}}, \overline{u_{h0}})$ by solving the system

$$A_c(\overline{n}_0^k)\overline{T_{c0}}^{k'} = f_c(\overline{n}_0^k, \overline{T_{L0}}^k, \overline{u_{e0}}^k, \overline{u_{h0}}^k), \tag{34}$$

where

$$(A_c)_{ij} = \begin{cases} -2\phi_1/\Delta x^2 - \nu(\overline{n}_0)_i^k & \text{if } i = j, \\ \phi_1/\Delta x^2 & \text{if } |i-j| = 1, \end{cases} \tag{35}$$

and

$$(f_c)_i(\overline{n}_0^k, \overline{u_{e0}}^k, \overline{u_{h0}}^k) = -\phi_2(\overline{n}_0)_i^k\left((\overline{u_{e0}})_i^k)^2 - \frac{\nu}{2}\left((\overline{u_{e0}})_i^k)^2 - ((\overline{u_{h0}})_i^k)^2\right)\right) - \nu(\overline{n}_0)_i^k(\overline{T_{L0}})_i^k, \tag{36}$$

obtaining the kth iteration step for the input variables $\overline{T_{c0}}$ and $\overline{V}_0$.

After evaluating the error between the input and the output variables, the real next step is chosen by using a relaxation parameter, θ, that helps to obtain a slower transition into the real solution and therefore prevents following iteration steps to diverge due to instabilities.

$$\overline{V}_0^{(k+1)} = \overline{V}_0^k + \theta(\overline{V}_0^{k'} - \overline{V}_0^k), \tag{37}$$

$$\overline{T}_{c0}^{(k+1)} = \overline{T}_{c0}^k + \theta(\overline{T}_{c0}^{k'} - \overline{T}_{c0}^k). \tag{38}$$

3 Results and discussion

3.1 Hot-carrier effects on a GaAs PN junction solar cell

In order to study the temperatures of charge carriers and lattice as separated variables, three different applied voltages (V_{ap}^*) were imposed on an illuminated non-symmetric junction ($x_J = L/10$). In Figs. 2 and 3, we

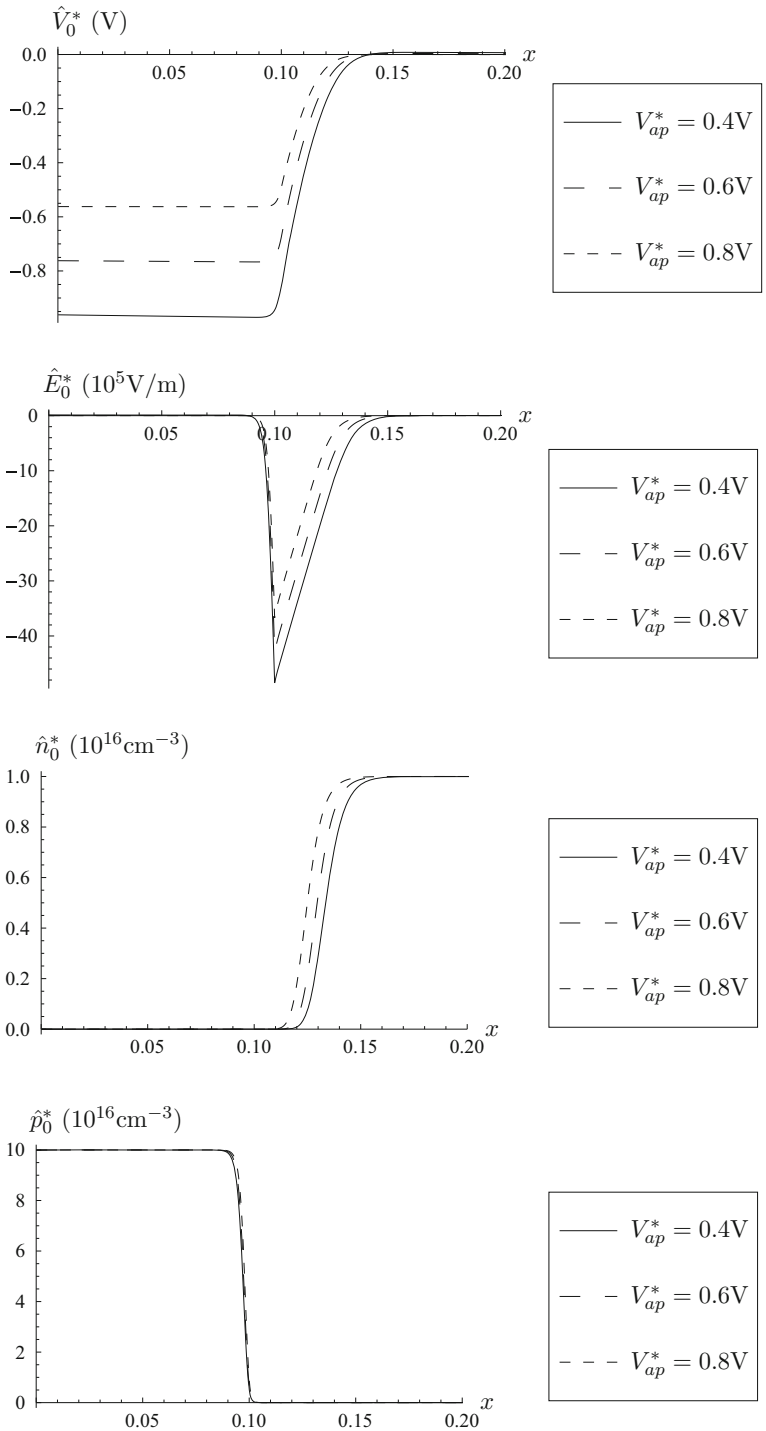

Fig. 2 Steady-state solution for a PN junction at different forward bias under light with $\alpha = 1403$, $R_e = 1.3 \times 10^{-3}$ and AM 1.5

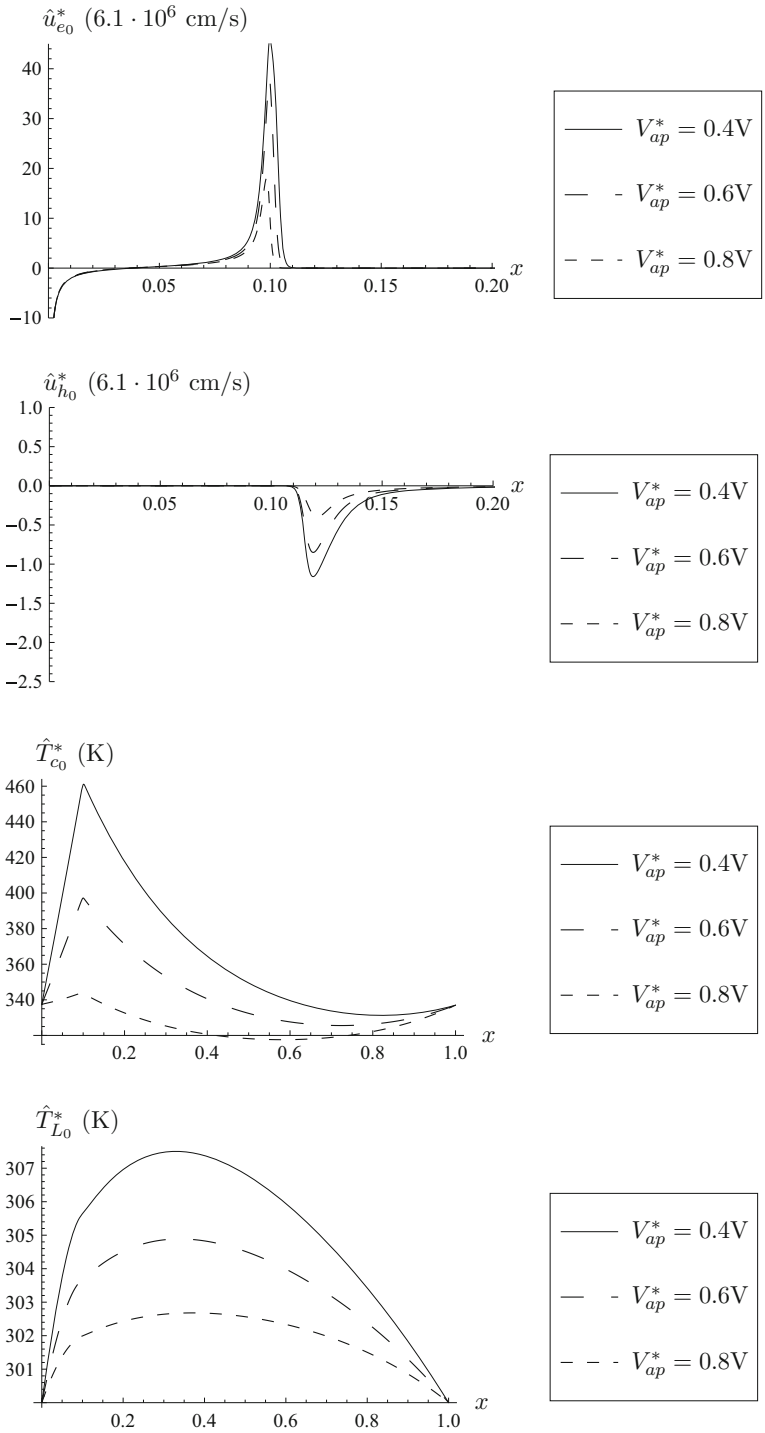

Fig. 3 Steady-state solution for a PN junction at different forward bias under light with $\alpha = 1403$, $R_e = 1.3 \times 10^{-3}$ and AM 1.5

show the region with the most abrupt changes for the variables through the device. This region corresponds to the neighborhood of the junction, while in the outside region ($x > 0.2$) there are no significant changes and variables asymptotically take the boundary conditions values. Results for voltage, electric field, electron density and hole density are shown in Fig. 2; and results for electron velocity, hole velocity, carrier temperature and lattice temperature are shown in Fig. 3. From these figures, voltage, electron density and hole density vary smoothly in space for the three applied biases. The maximum electron velocity is in the P-side, and the

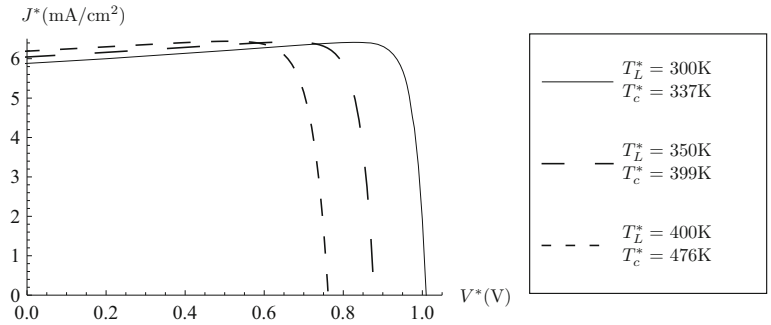

Fig. 4 Total current density–voltage characteristics for a GaAs PN junction solar cell under light with $\alpha = 3$, $R_e = 1.3 \times 10^{-3}$, AM 1.5, at different lattice temperature boundary conditions, T_L^*, and different charge carrier temperatures, T_c^*

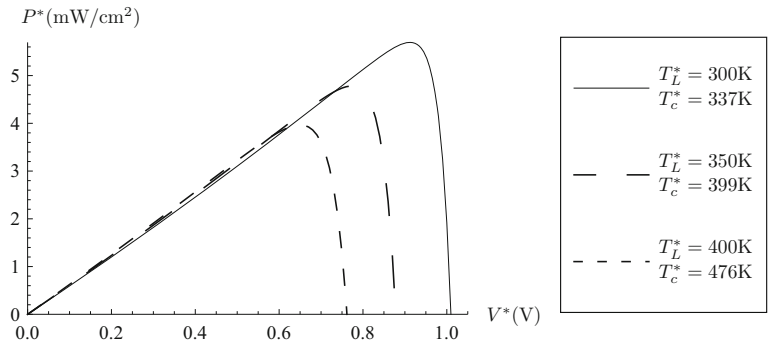

Fig. 5 Power output for a GaAs PN junction solar cell under light with $\alpha = 1403$, $R_e = 1.3 \times 10^{-3}$, AM 1.5, at different lattice temperature boundary conditions, T_L^*, and different charge carrier temperatures, T_c^*

maximum hole velocity is in the N-side. The maximum electron temperature is in the junction and decreases when the applied bias increases, and the lattice remains practically constant through the junction. The maximum absolute value of the electron and hole velocities decreases when the applied bias increases. These maximum values can be explained by the carrier temperature distribution through the junction.

Differences between lattice and carrier temperatures are expected to affect the performance of GaAs PN junction solar cells. By imposing specific boundary conditions for T_c, the performance of a solar cell under light is analyzed. Results in Figs. 4 and 6 show different curves for total current densities as a function of applied voltage for different boundary values of T_c and T_L. The net generation rate is obtained using Air Mass 1.5 ($AM1.5$), and Figs. 5 and 7 show the power output. The AM 1.5 spectrum corresponds to the sun being at an angle of elevation of 42 ^{o}, where the atmospheric thickness attenuates the solar spectrum to an integrated irradiance of $1000\,\mathrm{W/m^2}$. The maximum current and power output increase when the imposed carrier temperature boundary condition increases. This can be explained by favorable conditions for hot-carrier flow and can be physically achieved using energy selective contacts for reducing the carrier cooling rate. Quantum wells, quantum wires and quantum dots have been proposed to be used with this purpose [24].

3.2 GaAs solar cell characteristics and comparison to experimental data

Applied bias and doping density define the size of the region where the most abrupt changes in carrier densities, electrostatic potential and electric field distributions are taking place, and therefore provide the information of the conduction and valence band bending in the region around the junction. The voltage–current density characteristics in a GaAs PN junction solar cell with non-symmetric doping concentrations and sides, and with recombination and generation process, was studied with the one-dimensional two-temperature hydrodynamic model. The physical properties were obtained from Table 1 and the system parameters from Table 2.

Examples of calculated voltage–current density characteristics are shown in Figs. 4 and 6. The two-temperature hydrodynamic model predicts voltage–current characteristics showing a good agreement with measurements when the charge carrier temperature is higher than the lattice temperature, as shown in Figs. 4

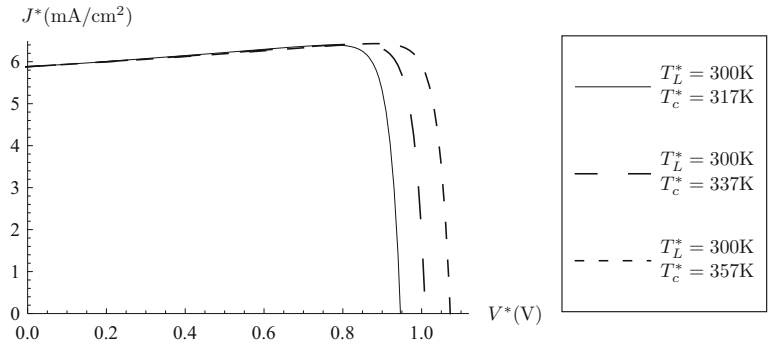

Fig. 6 Total current density–voltage characteristics for a GaAs PN junction solar cell under light with $\alpha = 3$, $R_e = 1.3 \times 10^{-3}$, AM 1.5, $T_L^* = 300\mathrm{K}$ (lattice temperature boundary conditions) at different charge carrier temperatures, T_c^*

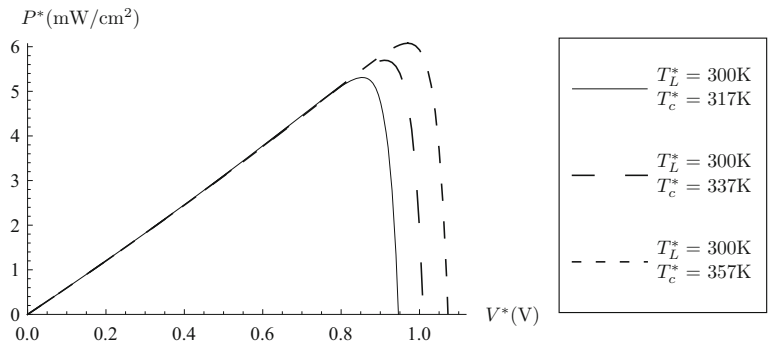

Fig. 7 Power output for a GaAs PN junction solar cell under light with $\alpha = 1403$, $R_e = 1.3 \times 10^{-3}$, AM 1.5, $T_L^* = 300\mathrm{K}$ (lattice temperature boundary conditions) at different charge carrier temperatures, T_c^*

and 6. When the charge carriers heat up and the lattice temperature boundary conditions remain constant, the power output increases as shown in Fig. 7. This is in agreement with hot electron devices [25]. The open-circuit voltage, V_{oc}, decreases and the short-circuit current, J_{sc}, increases when the cell temperature, T_L^*, increases [26]. The open-circuit voltage is in the order of 1 V at $T_L^* = 300\,\mathrm{K}$, 0.88 V at $T_L^* = 350\,\mathrm{K}$, and 0.76 V at $T_L^* = 400\,\mathrm{K}$, and increases when illumination intensity increases [27]. The predicted V_{oc} temperature coefficient (dV_{oc}/dT) is approximately $-2\mathrm{mV}/^\circ C$ as previously reported [27,28].

3.3 Reynolds number and viscous effects

The effects of carrier temperatures, device length and scattering effects in the total current densities through a GaAs PN junction solar cell were studied. The non-dimensional generation and recombination rates can be written as $G_n - R_n = \alpha\eta(G_n^* - R_n^*)$ and $G_p - R_p = \alpha\eta(G_p^* - R_p^*)$, with $\eta = m_e\varepsilon_s/N_0^2e^2\tau_{el}$. Therefore, variations in α can be considered to play a major role in variations of the non-dimensional net generation rate $G = G_n - R_n = G_p - R_p$. In the one-dimensional hydrodynamic model, the non-dimensional number α takes into account the variations in device length. The Reynolds number R_e and η take into account the scattering effects through the momentum relaxation time for electrons τ_{el}. If the momentum relaxation time for electrons decreases at constant device length, non-dimensional net generation rate increases and therefore total current increases. The Reynolds number can be written as $R_e = UL/(L^2/\tau_{el})$ where, in analogy with fluid mechanics, UL represents the inertial effects and (L^2/τ_{el}) represents the kinematic viscosity of the electron flow. By increasing the device length, L (α increases), the viscous effects increase and diffusion of carriers is modified through the junction, the electron and hole distributions are smoother at both edges of the junction, the electrostatic potential distribution is smoother, and the electric field distribution becomes sharper. In larger devices with a very short momentum relaxation time, most of the diffusion processes of carriers are taking place in a small region around the junction. This can contribute to the thermal diffusion and heat dissipation at the edges of the device, leading to have lower carrier temperatures.

3.4 Suggested improvements in design of solar cell

The power output of a solar cell can be increased by increasing the open-circuit voltage, V_{oc}, and the short-circuit current, J_{sc}. V_{oc} and J_{sc} depend on operational conditions such as lattice temperature, charge carrier temperature and light intensity, as well as device characteristics such as device length and doping densities. The temperature characteristic of V_{oc} is influenced by the temperature characteristic of saturation current. This current is proportional to the square root of the ratio between the diffusion constant and lifetime of electrons, which is usually represented by a power-law lattice temperature dependence, $T_L^{*\phi}$, with ϕ constant [29]. In the two-temperature hydrodynamic model, this ratio is proportional to the carrier temperature, T_c^*. Consequently, the charge carrier temperature plays a fundamental role in the predicted value of V_{oc}, and this suggests that some improvements can be done.

According to the results, when the lattice temperature remains constant, V_{oc} increases with the charge carrier temperature, as shown in Fig. 6. This can be achieved using contacts at both edges of the PN junction with a high electronic thermal conductivity in order to prevent charge carrier temperature fluctuations and avoid the heat dissipation of the photogenerated carriers into the lattice. On the other hand, lattice temperature boundary conditions are determined by lattice thermal conductivity as well as thermal properties of encapsulating layers in a PV module. Therefore, the metal contacts and encapsulating layers have to be designed to dissipate the heat from hot charge carriers in a sufficiently large region away from the contact–semiconductor interface, in order to operate the solar cell at lower lattice temperatures.

4 Conclusions

Carrier temperature boundary conditions affect the performance of the solar cell. Generated hot carriers at both edges of the device provide conditions to increase the total current density and power output. Under this condition, a higher applied bias reduces the maximum carrier temperature through the device and lattice temperature remains practically constant. A lower applied bias increases the maximum carrier temperature. According to this, the flow of hot carriers with a lower temperature variation through the device contributes more effectively to increase the electrical performance of a cell. At the same time, operating conditions with hot carriers with a much higher temperature than the lattice increase the total current density and power output and, consequently, improve the electrical performance of a GaAs PN junction solar cell.

The two-temperature thermal modeling contributes to predict the thermal resistance of solar cells and to improve the thermal control strategies and the design of cooling systems to be used in photovoltaic modules.

Acknowledgments We are grateful to Debdeep Jena for valuable discussions and FONDECYT Project 11110235 (Chile) for financial support, and Mr. Jara-Bravo would also like to thank a fellowship from CONICYT.

References

1. Royne, A., Dey, C.J., Mills, D.R.: Cooling of photovoltaic cells under concentrated illumination: a critical review. Sol. Energy Mater. Sol. Cells **86**, 451–483 (2005)
2. De Vos, A.: Detailed balance limit of the efficiency of tandem solar cells. J. Appl. Phys. **13**, 839–846 (1980)
3. Luque, A., Marti, A.: Theoretical limits of photovoltaic energy conversion. In: Handbook of Photovoltaic Science and Engineering, Wiley (2011)
4. Shur, M.: Introduction to Electronic Devices. Wiley, New York (1996)
5. Sze, S.M.: Semiconductor Devices, Physics and Technology. Wiley, New York (2002)
6. Lin, A.S., Phillips, J.D.: Drift–diffusion modeling for impurity photovoltaic devices. IEEE Trans. Electron Devices **56**, 3168–3174 (2009)
7. Nelson, J.: The Physics of Solar Cells. Imperial College Press, London (2003)
8. Blotekjaer, K.: Transport equations for electrons in two-valley semiconductors. IEEE Trans. Electron Devices **17**, 38–47 (1970)
9. Majumdar, A., Fushinobu, K., Hijikata, K.: Effect of gate voltage on hot-electron and hot-phonon interaction and transport in a submicrometer transistor. J. Appl. Phys. **77**, 6686–6694 (1995)
10. Ballestra, L., Micheletti, S., Sacco, R.: Semiconductor device simulation using a viscous-hydrodynamic model. Comput. Methods Appl. Mech. Eng. **191**, 5447–5466 (2002)
11. Jüngel, A., Tang, S.: A relaxation scheme for the hydrodynamic equations for semiconductors. Appl. Numer. Math. **43**, 229–252 (2002)
12. de Falco, C., Sacco, R., Scrofani, G.: Stabilized 3D finite elements for the numerical solution of the Navier-Stokes equations in semiconductors. Compu. Methods Appl. Mech. Eng. **196**, 1729–1744 (2007)

13. Romano, V., Rusakov, A.: 2d numerical simulations of an electron–phonon hydrodynamical model based on the maximum entropy principle. Comput. Methods Appl. Mech. Eng. **199**, 2741–2751 (2010)
14. Calderón-Muñoz, W., Sen M., Jena D.: Hydrodynamic instability of one-dimensional electron flow in ungated semiconductors. J. Appl. Phys. **102**, 0237034 (2007)
15. Calderón-Muñoz, W., Jena, D., Sen, M.: Hydrodynamic instability of confined two-dimensional electron flow in semiconductors. J. Appl. Phys. **106**, 0145064 (2009)
16. Abrarov, R.M., Sherman, E.Y., Sipe, J.E.: Hydrodynamic model for relaxation of optically injected currents in quantum wells. Appl. Phys. Lett. **91**, 232113 (2007)
17. Sherman, E.T., Abrarov, R.M., Sipe, J.E.: Dynamics of optically injected two-dimensional currents. J. Appl. Phys. **104**, 103701 (2008)
18. Mohseni, K., Shakouri, A., Ranm, R.J., Abraham, M.C.: Electron vortices in semiconductors devices. Phys. Fluids **17**, 100602 (2005)
19. Chen, G.: Potential-step amplified nonequilibrium thermal-electric converters. J. Appl. Phys. **97**, 1–9 (2005)
20. Calderón-Muñoz, W., Jena, D., Sen, M.: Thermal influence on hydrodynamic instabilities in a one-dimensional electron flow in semiconductors. J. Appl. Phys. **107**, 0745044 (2010)
21. Osses-Márquez, J., Calderón-Muñoz, W.: Thermal influence on charge carrier transport in solar cells based on GaAs PN junctions. J. Appl. Phys. **116**, 154502 (2014)
22. Kim, J.P., Lim, H., Song, J.H., Chang, Y.J., Jeon, C.H.: Numerical analysis on the thermal characteristics of photovoltaic module with ambient temperature variation. Sol. Energy Mater. Sol. Cells **95**, 404–407 (2011)
23. Holmes, M.H.: Introduction to Perturbation Methods. Springer, New York (1995)
24. Goodnick, S.M., Honsberg, C.: Ultrafast carrier relaxation and nonequilibrium phonons in hot carrier solar cells. In: Photovoltaic Specialists Conference (PVSC) IEEE, 2011 37th IEEE, 002066–002070, (2011)
25. Beard, M.C., Ellingson, R.J.: Multiple exciton generation in semiconductor nanocrystals: toward efficient solar energy conversion. Laser Photon. Rev. **25**, 377–399 (2008)
26. Bissels, G.M.M.W., Asselbergs, M.A.H., Bauhuis, G.J., Mulder, P., Haverkamp, E.J., Vlieg, E., Schermer, J.J.: Anomalous IV-characteristics of a GaAs solar cell under high irradiance. Sol. Energy Mater. Sol. Cells **104**, 97–101 (2012)
27. Nishioka, K., Takamoto, T., Agui, T., Kaneiwa, M., Uraoka, Y., Fuyuki, T.: Evaluation of temperature characteristics of high-efficiency InGaP/InGaAs/Ge triple-junction solar cells under concentration. Sol. Energy Mater. Sol. Cells **85**, 429–436 (2005)
28. Feteha, M.Y., Eldallal, G.M.: The effects of temperature and light concentration on the GaInP/GaAs multijunction solar cells performance. Renew. Energy **28**, 1097–1104 (2003)
29. Nishioka, K., Takamoto, T., Agui, T., Kaneiwa, M., Uraoka, Y., Fuyuki, T.: Annual output estimation of concentrator photovoltaic systems using high-efficiency InGaP/InGaAs/Ge triple-junction solar cells based on experimental solar cells characteristics and field-test meteorological data. Sol. Energy Mater. Sol. Cells **90**, 57–67 (2006)